CONSTRUCTION OF ELLIPSOIDAL PARTICLE DISCRETE ELEMENT MODEL AND CALIBRATION OF SIMULATION PARAMETERS
/
类椭球形状颗粒离散元模型构建与仿真参数标定

Zhiming WANG[1)], Zhanfeng HOU[*1,2,3)], Liyang BAO[1)], Yishuai LIU[1)], Bingyan LI[1)], Fang GUO[1)]
[1)] Inner Mongolia Agricultural University, College of Mechanical and Electrical Engineering, Inner Mongolia, China
[2)]Inner Mongolia Engineering Research Center of Intelligent Equipment for the Entire Process of Forage and Feed Production, Hohhot, 010018, China;
[3)]Inner Mongolia Engineering Research Center for Intelligent Facilities in Prataculture and Livestock Breeding, Hohhot 010018, China
Tel: +86-0471-4309215; E-mail: njau-hzf@163.com
Corresponding author: Zhanfeng Hou
DOI: https://doi.org/10.35633/inmateh-77-108

Keywords: *Forage seeds, Hyperspherical Model, Combination ball model, DEM*

ABSTRACT
To optimize the simulation process of seed pellet coating, this study employs the discrete element method to precisely model and analyze particles, using ice grass seeds as the research subject. The key procedures include constructing a three-dimensional pseudo-ellipsoidal geometric model based on the hyperquadratic surface pseudo-ellipsoid equation and defining it as the mesh division range for the DEM model. The Hertz–Mindlin with JKR contact model was selected to describe inter-particle interactions. A standardized filling sphere addition method for the ellipsoidal model was proposed. Using a central maximum filling sphere with a diameter of 1.2 mm as the baseline, composite models consisting of 17, 9, and 5 spheres were constructed with sphere diameters equal to 0.25, 0.5, and 0.75 times the baseline diameter, respectively. The filling sphere size corresponds to the largest inscribed sphere tangent to the ellipsoid. Through static angle of repose simulation tests, the optimal parameter combination was determined to achieve a target value of 30.54°, resulting in a shear modulus of 1.9 × 10⁷ Pa, a collision restitution coefficient of 0.5 for ice grass seeds, and a filling sphere diameter multiplier of 0.35. Under these conditions, the simulated static angle of repose averaged 30.67°, with a relative error of only 0.43%. Further dynamic calibration tests were conducted using a rotating drum. With a filling rate of 40%, a rotational speed of 58 r/min, and a simulation duration of 10 s, the simulated dynamic angle of repose was 38.12°, exhibiting a relative error of 0.88% compared with the physical test value of 38.46°. These results provide a valuable reference for discrete element modeling and parameter calibration of ellipsoidal particles.

摘要
为优化草种丸粒化包衣仿真过程，本研究以冰草种子为对象，应用离散元法对颗粒进行精确地建模和分析。主要内容为基于超二次曲面超椭球方程构建类椭球三维几何模型，并将其设为离散元模型的网格划分范围，选择"Hertz–Mindlin with JKR"接触模型，提出类椭球模型标准化填充球添加方式：以中心 1.2mm 最大填充球为基准，按其直径的 0.25、0.5、0.75 倍分别构建 17 球、9 球、5 球模型，其填充球大小为椭圆相切的最大内切球。通过休止角仿真试验，以 30.54°为目标值优化得到最佳参数组合剪切模量 1.9×10^7Pa、冰草种子间碰撞恢复系数 0.5、填充球直径倍数 0.35，此时仿真静态休止角均值 30.67°，相对误差仅 0.43%；旋转鼓动态标定试验中，旋转鼓的填充率为 40%、转速为 58r/min、仿真时长为 10s，仿真动态休止角 38.12°，与物理试验值 38.46°的相对误差为 0.88%。研究结果可为类椭球颗粒离散元建模提供参考。

INTRODUCTION
Granule coating technology, as a key process in pharmaceuticals *(Xiong et al., 2022; Deng et al., 2023)*, agriculture *(Liu et al., 2025; Wang et al., 2024; Li et al., 2025)*, and chemical engineering *(Pasha et al., 2017)*, plays a crucial supporting role in the ecological restoration of degraded grasslands through seed granule coating. The particle model employed during grass seed pelletization and coating has a significant influence on simulation accuracy and computational efficiency, making the development of an accurate discrete element model essential. Discrete element simulation, as a numerical method based on the mechanical behavior of particulate systems, is capable of describing complex particle interactions and provides a solid theoretical foundation for the pelletization and coating process. The Discrete Element Method (DEM) *(*Weston *et al., 2025; Hou et al., 2020)* not only accurately represents seed morphology at the microscopic scale and simulates particle trajectories and collision mechanisms, but also overcomes the limitations of traditional macroscopic experimental approaches in capturing micro-dynamic behaviors, thereby offering strong theoretical support for grass seed pelletization and coating technology.

How to accurately represent the geometric shape of particles is a key issue in discrete element method (DEM) analysis. In DEM simulations, particle models are generally classified into two major categories: spherical and aspherical. Aspherical particle models can be further divided into multi-sphere (clumped) models, superellipsoidal models, and polyhedral models.Currently, *Yang et al. (2023)* proposed a novel combinatorial modeling method to optimize the geometric model of garlic seeds, providing a more accurate modeling approach for irregularly shaped materials in DEM. *Liu et al. (2016)* established a three-dimensional DEM model of rice based on the theory of particle aggregates. By comparing simulation results with the natural repose angle of actual rice seeds, they verified the validity and feasibility of the 3D laser-scanned DEM model. *Qin et al. (2025)* calibrated the contact parameters between tobacco shreds and the porosity of the tobacco shred pile after drying, using the experimentally measured angle of repose as the optimal target value. *Li et al. (2025)* established a three-layer gradient adhesion mechanics model based on the mechanical properties of corn cob material, and proposed a “matrix coordinate positioning method” to achieve an equidistant topological distribution of corn kernels within the spatial structure of the cob, thereby completing the construction of a refined composite digital twin model for high-moisture corn cobs. *Bai et al. (2024)* proposed a triaxial spatial coordinate method and constructed a double-layer bonded DEM model of quinoa seeds, consisting of an epidermal layer and an endosperm layer. Through simulated compression tests, they optimized and calibrated the interparticle bonding parameters—including normal stiffness, tangential stiffness, and critical bonding moment—ultimately establishing a DEM model capable of accurately representing the mechanical characteristics of quinoa seeds. *Li et al. (2023)* developed two types of buckwheat seed particle models based on manual and automatic multi-sphere filling methods. Static and dynamic simulation tests showed that both the manually filled 7-sphere model and the automatically generated 36-sphere model achieved high simulation accuracy. *Chen et al. (2025)* constructed four representative samples of soybean mixtures using a default sphere-filling method. Based on numerical simulations of the soybean cleaning process, the optimal parameter combination for air-flow soybean winnowing equipment was determined.

In the field of discrete element simulation modeling, the composite sphere model is the predominant approach for constructing discrete element model systems. During the granular filling process, researchers commonly adopt automated filling algorithms or manual, experience-based filling strategies to assemble particle models. However, existing studies have not yet systematically investigated filling-sphere addition methods specifically tailored to composite sphere particle systems. Consequently, in-depth research on the scientific validity, rationality, and optimization strategies of these methods remains limited, and significant knowledge gaps persist regarding key parameters, including filling-sphere addition rules, particle size distribution, and filling efficiency.

To address the aforementioned issues, this study proposes a standardized sphere-packing method for ellipsoidal particles, using ice grass seeds as a representative case. By establishing a mapping relationship between geometric feature parameters and sphere distribution patterns, the proposed method enables precise discrete element modeling of irregular ellipsoidal particle systems. Using the angle of repose as the target response, optimal combinations of simulation parameters were determined through numerical experiments. Subsequently, stacking and rotating drum tests were conducted, and two-sample t-tests were applied to the static and dynamic angles of repose, respectively, to verify the reliability and accuracy of the simulation results.

EXPERIMENTAL METHODS

Description of Particle Geometric Shape

In practice, the dimensions of particles generally differ along each principal direction. The particle size can be described using the aspect ratio α *(Chen et al., 2005; Zhang et al., 2019)*, as defined in equation (1). Figure 1 illustrates the maximum chord length and the minimum side length of a particle.

$$\alpha = \frac{L}{W} \tag{1}$$

In the formula, L is the maximum chord length of the particle projection (mm), and W is the minimum side length corresponding to the maximum chord direction (mm).

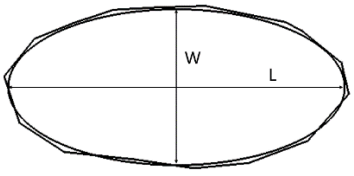

Fig. 1 - Schematic diagram of the maximum chord length and short side length of the particle

With further in-depth research, the concepts of particle sphericity α and the shape index were also proposed *(Xu et al., 2002)*, as shown in Equation (2).

$$\alpha = \frac{V_g}{V_B} \tag{2}$$

In the formula, V_g is the natural volume of the particle, in mm³; V_B is the volume of the particle as a sphere, in mm³. The sphericity α of the particle ranges from 0 to 1. The larger the sphericity α, the closer the particle shape is to a sphere. The smaller the sphericity α, the closer the particle shape is to a needle or flake.

Methods for Identifying Particle Geometry

Based on a comprehensive review of the current research, there is no unified standard for the classification of particle shapes *(Kong et al., 2011)*. In studies, two main approaches are commonly used to evaluate particle shapes: one is a general shape model based on mathematical modeling, where structures are characterized by describing features and categorized into four main types: circular, quasi-square, quasi-triangular, and quasi-elliptical; the other is shape recognition based on visual perception by the human eye, which identifies a more diverse range of forms.

The range of shapes that human visual cognition can recognize is extremely broad. In the visual perception system, shape, as a core element of object recognition, plays a key role in constructing the cognitive framework of object shapes. Taking common forage seeds as an example, such as agropyron seeds, oat seeds, red clover seeds, and alfalfa seeds, their shapes can be roughly categorized as ellipsoidal, domed cylindrical, and kidney-shaped from a geometric feature perspective, with the specific details shown in Table 1.

Table 1

Description of the shapes of the different seeds

Forage seeds	Physical shape	Similar shapes
Agropyron seeds		Ellipsoid-like shape
Oat seeds		Ellipsoid-like shape
Red clover seeds		Domed Cylindrical
Alfalfa Seeds		Kidney-shaped

In the above context, the geometric characteristics of ice grass seeds gradually emerge. By observing and analyzing the seed's shape, it can be found that its overall form is ellipsoid-like. For this ellipsoid-like geometric model, this study proposes a broadly applicable combined sphere model filling method. This method not only simplifies the model construction process but also significantly improves the computational efficiency and accuracy of simulations, providing a reference for subsequent coating process simulation and analysis.

Geometric Model Construction Based on Superquadric Equations

This study aims to enhance the accuracy and efficiency of forage seed modeling by proposing a superellipsoid-based approach to construct the shell framework, which serves as the mesh division boundary for the composite sphere model. Provides precise and efficient modeling solutions for the micro-mechanics simulation of forage seeds.

Using the hyperellipsoidal equation (3) for a hyperquadric surface as a reference, a three-dimensional hyperellipsoidal model was established in CATIA. The resulting hyperellipsoidal equation (4) generated using CATIA software is:

$$f(x,\ y,\ z) = \left(\left| \frac{x}{a} \right|^{s_2} + \left| \frac{y}{b} \right|^{s_2} \right)^{\frac{s_1}{s_2}} + \left| \frac{z}{c} \right|^{s_1} = 0 \tag{3}$$

$$f(x,\ y,\ z) = \left(\left| \frac{x}{a} \right|^{\frac{1}{1-s_2}} + \left| \frac{y}{b} \right|^{\frac{1}{1-s_2}} \right)^{\frac{1-s_1}{1-s_2}} + \left| \frac{z}{c} \right|^{\frac{1}{1-s_1}} = 0 \tag{4}$$

In the equation, a, b, and c control the scale (equivalent to radius) in the x, y, and z directions, respectively, in mm; s_1 and s_2 are shape indices, where s_1 governs the shape in the z direction and s_2 determines the shape within the xoy plane.

By modifying the five parameters a, b, c, s_1, and s_2 in equation (4), the hyperellipsoid model can describe the shapes of most particles. Figure 2 shows non-spherical models generated in CATIA software by varying these five parameters.

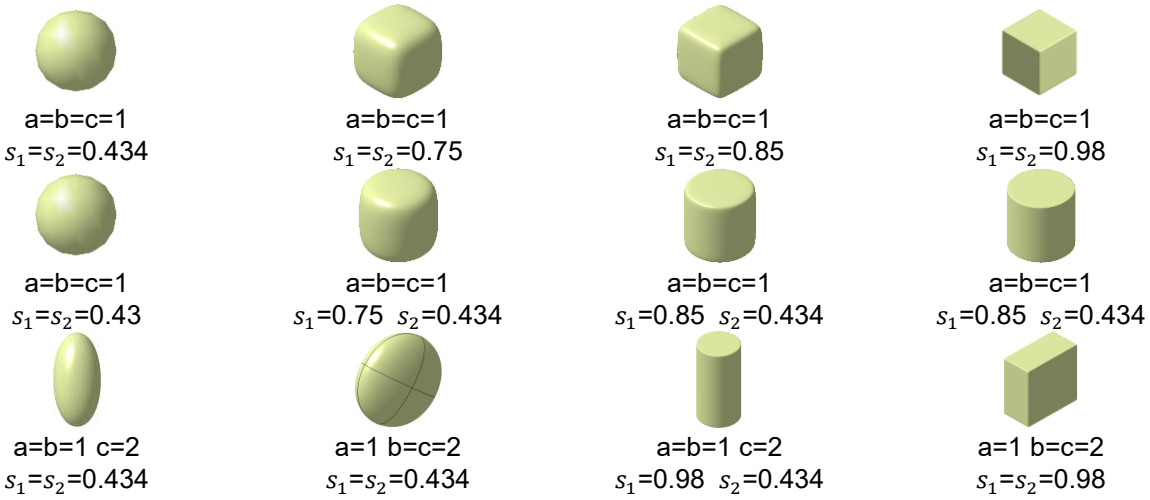

Fig. 2 - Non-spherical particles obtained by the superellipsoid model

The shape index is a key parameter for quantitatively characterizing the deviation of a hyperellipsoid from a standard ellipsoid. It directly influences the sharpness of the hyperellipsoid's edges and its overall contour, serving as a critical metric for achieving an accurate digital representation of seed geometry. As the shape index approaches 1, the hyperellipsoid exhibits pronounced right-angled edges; when it approaches 0.434, the edges become progressively rounded; and as it approaches 0, the profile approximates a straight line. According to the above modeling method, a discrete element model of forage seeds is Following the aforementioned modeling approach, a discrete element model of forage seeds was established based on their triaxial dimensions. Table 2 presents the forage seed model developed in this study along with reference values for shape indices.

Table 2

Shape index reference table

Forage seeds	Actual forage seeds	Forage Seed Model	Shape Index Reference Range	This article selects Shape Index
Agropyron seed			s_1: 0.17～0.28 s_2: 0.19～0.31	s_1=0.23 s_2=0.25
Red clover seeds			s_1: 0.18～0.27 s_2: 0.13～0.21	s_1=0.22 s_2=0.16

Method for Establishing the Composite Sphere Model

This study focuses on ice grass seeds. First, a hyperellipsoidal geometric model of the seeds was constructed using CATIA software and exported in STL format. The model was then imported into EDEM software, where its contour boundaries were used as the mesh division boundaries for the composite sphere model. During the sphere-filling process, the ice grass seed was equivalently simplified as an ellipsoid, with its length (L), width (W), and thickness (T) parameters corresponding to the actual seed dimensions. Based on the results of seed parameter calibration tests, a seed width of 1.2 mm was selected as the maximum filling-sphere diameter. This value represents the minimum lateral characteristic dimension of the seed, ensuring that all filling spheres are fully inscribed within the ellipsoidal contour and do not exceed the actual geometric boundaries of the seed. Using the maximum filling-sphere diameter D=1.2 mm as the reference, sphere diameters of 0.25D, 0.5D, and 0.75D were selected to construct discrete element models consisting of 17, 9, and 5 spheres, respectively.

The method for establishing the 17-ball model of ice grass seeds is as follows: The length, width, and thickness of the ice grass seed correspond to the Z-axis (axis Z), X-axis (axis X), and Y-axis (axis Y) of the

ellipsoid seed, respectively. At this point, N=17. To fill the 17-ball model, on the xoz plane, first place the largest inscribed sphere Omax (sphere O1) with diameter D=1.2mm at the ellipsoid's center point. Then, using 0.25 times the maximum filling sphere diameter as reference, sequentially add filling spheres at intervals of D/4×n, where n is an integer and n∈(0, (N-1)/2], where n is an integer representing the maximum inscribed sphere of the ellipse at that position. Subsequently, fill spheres are added at the ellipsoid's symmetrical positions (0, D/4) and (0, -D/4), with sizes matching the largest inscribed spheres at these points, i.e., spheres O2 and O3. Next, symmetrically add filling spheres at positions (0, D/2) and (0, -D/2), corresponding to spheres O4 and O5. Proceeding similarly, the final filling spheres are added at positions (0, 2D) and (0, -2D), corresponding to spheres O16 and O17, as shown in Figure 3. The above operations complete the filling construction of the 17-ball model.

The 9-ball composite model and the 5-ball composite model are filled using the aforementioned method. In the 9-ball composite model, when filling the farthest ball, if it remains the largest ellipsoidal inscribed sphere, balls O6 and O8 may not make contact. To prevent this, this experiment merges part of balls O6 and O8, as shown in Figures 4 and 5.

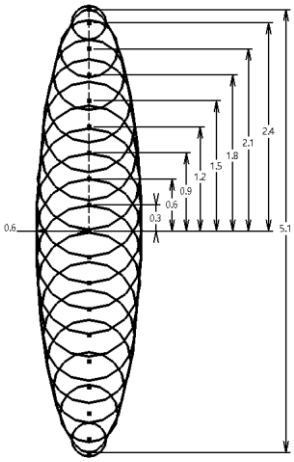

Fig. 3 - Model of 17 balls in combination

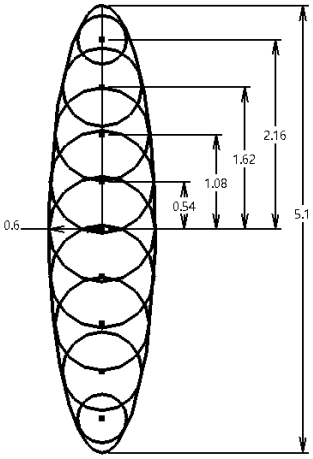

Fig. 4 - Combination ball 9-ball model

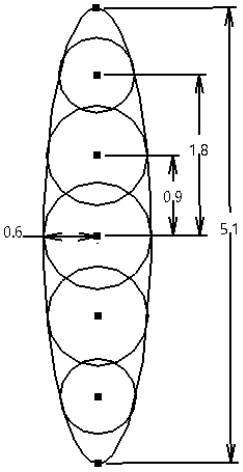

Fig. 5 - Combination ball 5-ball model

Simulation Parameters and Model

The test apparatus is an FT-104B angle of repose tester. A 1:1 scale model of the tester, created in CATIA software, was imported into EDEM software. The instrument's bore length is 28 mm, with the funnel inlet and outlet having inner diameters of 25 mm and 10 mm, respectively. A transparent disk with a radius of 50 mm and height of 5 mm was placed 40 mm below the angle of repose tester. The ice grass seed simulation model and angle of repose tester model are shown in Figure 7. A circular virtual particle factory was constructed at the top inlet of the funnel to generate ice grass seed particles. The particle generation mechanism employed a dynamic generation mode, achieving orderly seed particle generation and distribution through real-time computation and simulation. During the simulation, the particle factory generated a total of 1000 ice grass seeds over a simulation duration of 5 seconds. The time step size was set to 3.8×10^(-7), and the grid size was three times the minimum particle radius.

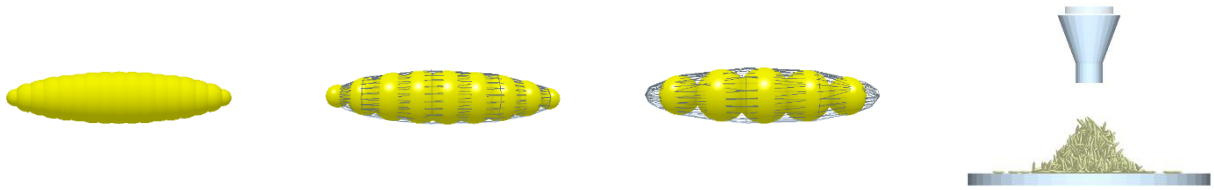

(a) 17 sphere model *(b) 9 sphere model* *(c) 5 sphere model* *(d) Angle of repose measurement model*

Fig. 7 - Combined sphere model and angle of repose determination model

SIMULATION EXPERIMENT DESIGN

Significance Analysis of Plackett-Burman Test

The parameters used in the numerical simulations were obtained from the research group's previous calibration studies *(Hou et al., 2020)*. In this study, a Plackett–Burman experimental design was employed to rapidly screen all investigated factors, enabling the identification of key factors that exert a significant influence on the target response while excluding minor factors with negligible effects.

The ranges of the selected parameters are listed in Table 3. After all particles had settled on the bottom disk and formed a stable conical pile, the angle of repose was calculated using MATLAB software.

Table3

Plackett-Burman test parameter range table

Test parameters	Low level (-1)	Hight level (+1)
Poisson's ratio of Agropyron seed As	0.3	0.5
Shear modulus of Agropyron seed Bs/MPa	5	20
Agropyron seed-Agropyron seed restitution coefficient Cs	0.45	0.65
Agropyron seed-Agropyron seed static friction coefficient Ds	0.5	0.7
Agropyron seed-Agropyron seed rolling friction coefficient Es	0.6	0.9
Agropyron seed-Steel plate restitution coefficient Fs	0.4	0.6
Agropyron seed-Steel plate static friction coefficient Gs	0.2	0.4
Agropyron seed-Steel plate rolling friction coefficient Hs	0.3	0.6
Maximum filled sphere diameter multiple Js	0.25	0.75

Steepest Ascent Experiment

Based on the Plackett–Burman design, steepest ascent experiments were conducted for the three significant parameters identified—shear modulus, coefficient of restitution between ice grass seeds, and the maximum packing ball diameter multiplier of the seeds. The relative error between the simulated and measured static angles of repose was used as the evaluation metric to determine the optimal range of simulation parameters *(Chen et al., 2025)*. Since the center distance multiplier was one of the significant influencing factors, models with 17 balls (0.25×), 11 balls (0.35×), 9 balls (0.45×), 7 balls (0.55× and 0.65×), and 5 balls (0.75×) were constructed, Figure 8 shows the remaining three models in addition to the three previously described models.

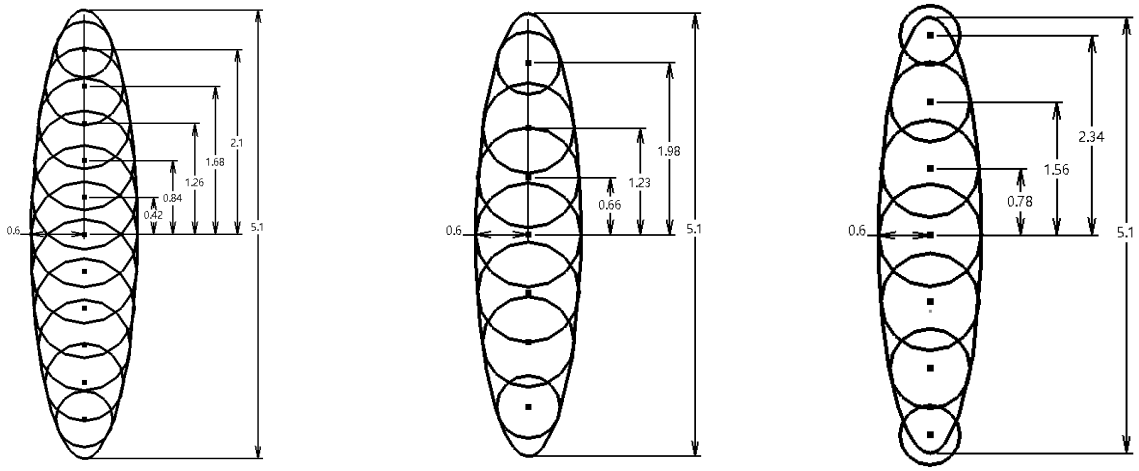

(a) 0.35D 11-ball model *(b) 0.55D 7-ball model* *(c) 0.65D 7-ball model*

Fig. 8 - Combined spherical model with different multiples

Box-Behnken Experimental Design

When conducting the Box–Behnken experimental design in Design-Expert, the significant factors were used as the basis for variable selection. The experimental parameters from the second group of the steepest ascent test were selected as the center point (coded as 0), while the parameters from the first and third groups corresponded to the low (−1) and high (+1) levels of the experiment, respectively. A quadratic regression model was established between the fitted factors and the response values to determine the optimal combination of parameters. The specific experimental design scheme is presented in Table 4. During the simulation, all non-significant factors were kept constant at the average values determined in the steepest ascent test.

Table 4

Box-Behnken Experimental Design Scheme

Level	Factor		
	Shear modulus of Agropyron seed	Agropyron seed-Agropyron seed restitution coefficient	Maximum filled sphere diameter multiple
+1	11	0.53	0.45
0	8	0.49	0.35
-1	5	0.45	0.25

Rotating Drum Test

The dynamic angle of repose refers to the stable angle formed between the surface of a granular material in motion (such as during drum rotation, conveying, or dumping) and the horizontal plane *(Jian et al., 2023)*. This parameter is widely used to characterize the dynamic flowability of particles and is crucial for evaluating material behavior in processes such as mixing, coating, and conveying. In this study, a combination of physical experiments and numerical simulation was employed to calibrate the dynamic angle of repose of ice plant seeds.

The rotational method was adopted, in which a rotating drum test was used to determine the dynamic angle of repose. Based on multiple preliminary trials, the drum rotation speed was set to 58 rpm, and the particle filling rate was maintained at approximately 40%. Flow images of the seeds inside the rotating drum were recorded using a high-speed camera.

RESULTS AND DISCUSSION

Results of the Plackett-Burman Test

The Plackett–Burman experimental design and corresponding results are presented in Table 5. Analysis of variance (ANOVA) was conducted on the experimental data using Design-Expert. As shown in Table 6, the P-values for the shear modulus and the coefficient of restitution for ice grass seed–seed collisions were both less than 0.05, indicating significant effects on the static angle of repose. The P-value for the maximum packing ball diameter multiplier of the seeds was less than 0.01, indicating a highly significant effect. The P-values for the remaining simulation parameters were all greater than 0.05, suggesting that their effects on the static angle of repose were statistically insignificant and could be largely disregarded. Consequently, these three parameters were identified as the primary factors influencing the packing behavior of ice grass seeds, providing a theoretical basis and parameter foundation for subsequent optimization modeling and simulation analysis.

Table 5

Plackett-Burman test protocol and results

No.	Experimental parameters									Repose angle θ/(°)
	As	Bs	Cs	Ds	Es	Fs	Gs	Hs	Js	
1	-1	1	1	-1	1	1	1	-1	-1	24.36
2	1	1	-1	1	1	1	-1	-1	-1	22.67
3	1	1	1	-1	-1	-1	1	-1	1	32.91
4	-1	-1	-1	-1	-1	-1	-1	-1	-1	26.56
5	-1	-1	-1	1	-1	1	1	-1	1	35.69
6	1	-1	1	1	1	-1	-1	-1	1	38.98
7	-1	1	1	1	-1	-1	-1	1	-1	24.69
8	-1	-1	1	-1	1	1	-1	1	1	33.69
9	-1	1	-1	1	1	-1	1	1	1	30
10	0	0	0	0	0	0	0	0	0	30.83
11	1	1	-1	-1	-1	1	-1	1	1	27.47
12	1	-1	1	1	-1	1	1	1	-1	30.63
13	1	1	-1	-1	1	-1	1	1	-1	23.82

Table 6

Significance analysis of Plackett-Burman test parameters

Parameters	Degree of freedom	Sum of squares	F-value	P-value
As	9	297.71	35.09	0.7011
Bs	1	0.185	0.1963	0.0149
Cs	1	61.97	65.74	0.0298
Ds	1	30.24	32.08	0.0542
Es	1	15.99	16.96	0.3184
Fs	1	1.64	1.73	0.5421
Gs	1	0.5002	0.5306	0.4242
Hs	1	0.9352	0.9921	0.0839
Js	1	9.85	10.45	0.0053

Note: **Indicates that the impact is extremely significant (P<0.01). and * Indicates that the impact is significant (P<0.05). The same below.

Steepest Climb Experiment Results

The design and results of the steepest ascent test are presented in Table 7. Test 2 exhibited the smallest

relative error, indicating that the optimal parameter range is likely located near this point. Accordingly, the parameter set from Test 2 was selected as the center point for the response surface experiment. Tests 1 and 3 were designated as the low and high levels, respectively, for constructing the subsequent Box–Behnken response surface optimization design. In the following simulation experiments, parameters that had insignificant effects on the response variables were fixed at the average values obtained from physical experiments. Specifically, the Poisson's ratio of ice grass seeds was set to 0.4; the static friction coefficient between seeds was 0.6, and the dynamic friction coefficient was 0.75. The coefficient of restitution between ice grass seeds and the coating pan was 0.49, while the static and rolling friction coefficients were set to 0.29 and 0.45, respectively.

Table 7

The steepest climbing test design scheme and results

No.	Shear modulus of Agropyron seed / (MPa)	Agropyron seed-Agropyron seed restitution coefficient	Maximum filled sphere diameter multiple	Repose angle θ / (°)	Relative error / %
1	5	0.45	0.25	35.08	14.87
2	8	0.49	0.35	30.62	0.26
3	11	0.53	0.45	28.18	7.72
4	14	0.57	0.55	26.22	14.11
5	17	0.61	0.65	36.71	20.2
6	20	0.65	0.75	32.83	7.5

Box-Behnken Test Results

Subsequently, a multivariate second-order regression analysis was conducted on the Box–Behnken experimental data using Design-Expert software. A second-order response surface regression model was established between the repose angle response values and the significant factors to describe the variation patterns of the simulation results. The resulting second-order regression equation is as follows:

$$\theta = 82.24 + 0.78A\mathrm{s} - 410.08B\mathrm{s} + 259.34I\mathrm{s} - 4.68A\mathrm{s}B\mathrm{s} + 0.43\mathrm{AsIs} - 134.9\mathrm{BsIs} + 0.05\mathrm{As}^2 + 470.9B\mathrm{s}^2 - 184.7I\mathrm{s}^2 \quad (5)$$

The analysis of variance results for the repose angle obtained from the Box–Behnken experimental design are shown in Table 8. The results indicate that the interaction terms As×Bs and Bs×Js, as well as the quadratic terms of the main effects As², Bs², and Js², all have extremely significant effects on the repose angle ($P < 0.01$). The main effects As, Bs, and Js are significant ($P < 0.05$), whereas the interaction term As×Js is not significant ($P > 0.05$). For the regression model of the repose angle, the overall P-value of the regression is less than 0.0001, indicating extremely high significance. The P-value for the lack-of-fit term is 0.8432 (> 0.05), suggesting that the model does not exhibit a significant lack of fit and therefore provides a good fit to the data. The coefficient of determination R^2 is 0.9794, and the adjusted R^2 is 0.9528, both of which are close to 1, indicating that the model has strong explanatory power. The coefficient of variation (CV) is 2.76%, demonstrating that the model possesses good stability and reliability. In summary, the regression model shows very high significance and excellent goodness of fit, and can accurately and effectively describe the variation pattern of the repose angle.

Table 8

Box-Behnken experiment design scheme and results

No.	Shear modulus of Agropyron seed/ (MPa)	Agropyron seed-Agropyron seed restitution coefficient	Maximum filled sphere diameter multiple	Repose angle θ/(°)
1	1.000	1.000	0.000	35.86
2	0.000	0.000	0.000	35.71
3	0.000	0.000	0.000	33.93
4	0.000	0.000	0.000	36.38
5	-1.000	0.000	1.000	28.73
6	0.000	-1.000	-1.000	25.19
7	0.000	1.000	1.000	22.98
8	-1.000	1.000	0.000	45.56
9	0.000	0.000	0.000	34.24
10	1.000	-1.000	0.000	45.55

No.	Shear modulus of Agropyron seed/ （MPa）	Agropyron seed-Agropyron seed restitution coefficient	Maximum filled sphere diameter multiple	Repose angle θ/(°)
11	1.000	0.000	-1.000	21.26
12	0.000	1.000	-1.000	27.39
13	0.000	0.000	0.000	31.2
14	0.000	-1.000	1.000	34.27
15	1.000	0.000	1.000	26.29
16	-1.000	-1.000	0.000	41.21
17	-1.000	0.000	-1.000	26.89

Table 9

Variation analysis of Box-Behnkentest quadratic model

Source of variance	Mean square	Degree of freedom	Sum of squares	P-value
Model	91.63	9	824.69	< 0.0001**
As	22.55	1	22.55	0.0245
Bs	26.03	1	26.03	0.0181
Js	16.65	1	16.65	0.0438
AsBs	49.28	1	49.28	0.0039
AsJs	2.54	1	2.54	0.3693
BsJs	45.5	1	45.5	0.0048
As^2	39.01	1	39.01	0.0071
Bs^2	93.37	1	93.37	0.0007
Js^2	561.06	1	561.06	<0.0001**
Residual	2.76	7	19.35	
Lack of fit	1.09	3	3.28	0.8432
Pure error	4.02	4	16.06	
Sum	844.04	16		

Note: **Indicates that the impact is extremely significant (P<0.01). and * Indicates that the impact is significant (P<0.05). The same below.

Determination of the Optimal Parameter Combination and Simulation Verification

Based on the second-order regression model (Equation (5)), the target static angle of repose was set to 30.54°. Multi-objective optimization was conducted using the Design-Expert optimization module to minimize the deviation between the simulated repose angle and the physically measured value (30.54°). Among the multiple candidate solutions generated, the parameter combination that most closely matched the average value obtained from the physical tests was selected as the optimal set for ice grass seed modeling. According to the optimization results, the significant influencing parameters were calibrated accordingly: the shear modulus was set to 1.9×10^7 Pa, the seed-to-seed coefficient of restitution to 0.5, and the maximum packing sphere diameter ratio to 0.35. Parameters that exhibited insignificant effects on the response variable were assigned the mean values obtained from the physical measurements.

To verify the reliability and accuracy of the calibrated parameters for the discrete element simulation of ice grass seeds, the optimized parameter set was imported into EDEM to conduct three independent replicate simulations. The resulting angles of repose were 28.11°, 32.19°, and 30.74°. A two-sample t-test was performed to assess whether a significant difference existed between the simulated and physically measured angles of repose. The test yielded P = 0.635 > 0.05, indicating that the difference between the two datasets was not statistically significant, and demonstrating strong agreement between the simulation and physical test results. The mean simulated angle of repose was 30.35°, with a relative error of 0.622% compared with the physical test average of 30.54°. These results further validate the rationality and effectiveness of the discrete element model and its calibrated parameter settings.

Rotating Drum Experiment Results

The simulation and physical test results are presented in Figures 9 and 10. From three repeated physical experiments, the measured dynamic angles of repose were 37.22°, 38.94°, and 39.21°, with an average of 38.46°. Using the parameters determined from the static angle calibration experiments, three discrete element simulations were conducted, yielding dynamic angles of repose of 37.42°, 38.21°, and 38.73°, with an average of 38.12°. The relative error compared with the physical test average was 0.88%. A two-sample t-test was performed between the simulated and physical dynamic angles of repose, yielding P = 0.466 > 0.05. These results indicate no significant difference between the simulation and physical test results, further validating the reliability of the discrete element model.

Fig. 9 - Physical experiment of dynamic angle of repose

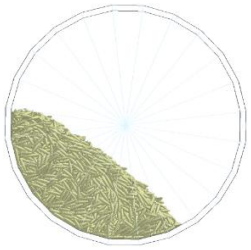

Fig. 10 - Simulation test of dynamic angle of repose of the combined ball

In comparison to manual empirical approaches and the automatic packing method implemented in EDEM, the modeling strategy proposed in this study effectively minimizes the number of spheres required for packing. By accurately specifying both the diameter and spatial arrangement of each sphere, the approach not only enhances the computational efficiency of discrete element simulations but also maintains simulation accuracy. In addition, it significantly improves overall modeling efficiency while reducing the time and resources needed for preliminary data processing and model construction.

CONCLUSIONS

This study proposes a parametric modeling method based on the hyperellipsoidal equation of a hyperquadric surface. Using the hyperellipsoid as the mesh boundary, a pseudo-ellipsoidal filling-sphere model was constructed. Based on this approach, composite sphere models with three different filling schemes were developed. The optimal filling configuration for the ice grass seed composite sphere model was determined to consist of 11 spheres with a scaling factor of 0.35, providing an efficient solution for geometric modeling in seed discrete element simulations.

Dynamic angle of repose calibration tests were conducted to validate the reliability of the proposed model. The experimentally measured angle of repose was 37.46°, while the average value obtained from three repeated simulation tests was 36.38°, resulting in a relative error of only 1.34%. A two-sample t-test yielded a P-value of 0.724 ($P > 0.05$), indicating no statistically significant difference between the experimental and simulated results. The validated model establishes a reliable foundation for analyzing seed motion characteristics in subsequent agricultural machinery operations. In addition, the proposed modeling framework facilitates the adaptation of filling parameters for different crop seeds, thereby enhancing the versatility and applicability of the discrete element model.

ACKNOWLEDGEMENT

The authors were funded for this project by the Development and Research on Key Technologies and Equipment for Degraded Grassland Restoration Based on Coated Forage Seed Hydroseeding (No. 2023YFDZ0006), the Science and Technology Research Project of Inner Mongolia Autonomous Region Higher Education Institutions (No.NJZZ23046), the Inner Mongolia Agricultural University Young Faculty Research Capacity Enhancement Program (BR220128), the Inner Mongolia Agricultural University High-Level Talent Recruitment and Research Start-up Program (NDY2022-56), and the Inner Mongolia Autonomous Region “First-Class Discipline Construction Special Program” (YLXKZX-NND-046).

REFERENCES

[1] Deng, S., Zhang, X., Zhang, J.,Zhang, J., Huo, B., Liu, H., (2023). Study on the uniformity of ellipsoidal tablet film coating process (椭球形片剂薄膜包衣均匀性工艺研究). *Tianjin Chemical Industry*, Vol. 37, pp.49-52. https://doi.org/10.3969/j.issn.1008-1267.2023.06.014

[2] Xiong, G., Su, W., Wang, A., Wang, Y., (2022). Numerical simulation of effect of particle shape on tablet particles motion characteristics in a pan coater (颗粒形状对包衣设备内药片颗粒运动特性影响的数值模拟). *Journal of Process Engineering*, Vol. 22, pp. 1232-1243. https://doi.org/10.12034/j.issn.1009-606X.221329

[3] Liu, H., Ma, X., Hou, Z., Chen, L., Tan, A., Liu, Y., (2025). Simulation and Experimental Study on the Optimization of Operating Parameters for Coating Pellets of Agropyron Seeds. *Agriculture*, Vol. 15, pp. 2017-2017. https://doi.org/10.3390/AGRICULTURE15192017

[4] Wang, X., Pi, N., Weng, Q., (2024). Research Progress of Seed Pelleting (种子丸粒化及其研究进展). *Hunan Agricultural Sciences*, No. 03, pp. 85-90. https://doi.org/10.16498/j.cnki.hnnykx.2024.003.018

[5] Li, C., (2025). Development Status of Seed Coating Technology and Its Impact on Crop Yield (种子包衣

技术的发展现状及其对作物产量的影响). *Seed Science and Technology*, Vol. 43, pp. 198-200. https://doi.org/10.19904/j.cnki.cn14-1160/s.2025.05.063

[6] Pasha, M., Hare, C., Ghadiri, M., Gunadi, A., Piccione, P., (2017) Inter-particle coating variability in a rotary batch seed coater. *Chemical Engineering Research and Design*, Vol. 120 pp. 92-101. https://doi.org/10.1016/j.cherd.2017.01.033.

[7] Weston, D., Cabiscol, R., Yule, W., Gobby, D., (2025). Discrete Element Method Contact Force Parameter Impact for Particle-Level Interactions in Agitated Mills. *Powder Technology*, Vol. 469, pp. 121728-121728. https://doi.org/10.1016/J.POWTEC.2025.121728

[8] Hou, Z., Qiu, Y., Chen, Z., Liu, H., Guo, F., Mi, L., (2020). Optimization of Process Parameters of Pelletizer for Agropyron Seeds under Vibration Force Field. *INMATEH-Agricultural Engineering*, Vol. 60, pp. 147-154. https://doi.org/10.35633/inmateh-60-17

[9] Yang, Q., Song, J., Zhang, M., Zhang, Y., Wang, Z., Li, K., (2023). Study on Discrete Element Modeling Method of Garlic Seeds (蒜种离散元建模方法的研究). *Journal of Shandong University of Technology (Natural Science Edition)*, Vol. 37, pp. 48-52. https://doi.org/10.13367/j.cnki.sdgc.2023.05.007

[10] Liu, C., Wang, Y., Song, J., Li, Y., Ma, T., (2016). Study on Discrete Element Modeling and Experiment of Rice Seeds Based on 3D Laser Scanning (基于三维激光扫描的水稻种子离散元建模及试验). *Transactions of the Chinese Society of Agricultural Engineering*, Vol. 32, pp. 294-300. https://doi.org/10.11975/j.issn.1002-6819.2016.15.041

[11] Qin, J., Li, Z., Zhao, B., Wang, Y., (2025). Calibration and Experiment of Contact Parameters of Tobacco Shreds in Discrete Element Model (烟丝于离散元模型中接触参数的标定与实验). *Agricultural Equipment & Vehicle Engineering*, Vol. 63, pp. 120-124. https://doi.org/10.3969/j.issn.1673-3142.2025.01.021

[12] Li, C., Liu, Z., Geng, L., Xu, T., Feng, W., Liu, M., Qiao, D., Wang, Y., Wang, J., (2025). The Establishment of a High-Moisture Corn Ear Model Based on the Discrete Element Method and the Calibration of Bonding Parameters. *Agriculture*, Vol. 15, pp. 752-752. https://doi.org/10.3390/AGRICULTURE15070752

[13] Bai, H., Wu, Y., Ma, Y., Xuan, D., Du, W., Liu, F., Zhao, X., (2024). Discrete Element Model Construction and Dehulling Simulation Verification Based on Harvested Quinoa Grains. *Journal of Food Science*, Vol. 89, pp. 9336-9353. https://doi.org/10.1111/1750-3841.17510

[14] Li, G., Li, H., Li, X., Gong, Z., Yang, Q., Huang, Y., Fu, Z., (2023). Establishment and Calibration of Discrete Element Model for Buckwheat Seed Based on Static and Dynamic Verification Test. *Agriculture*, Vol. 13. https://doi.org/10.3390/AGRICULTURE13051024

[15] Chen, G., Li, F., Qu, F., Zhang, C., (2025). Simulation study on soybean winnowing based on CFD–DEM coupling, *INMATEH - Agricultural Engineering*, Vol. 77, pp. 362-372. https://doi.org/10.35633/inmateh-77-29

[16] Chen, H., Wang, R., Li, J., Zhang, J., (2005). Analysis of Particle Shape of Calcareous Sand (钙质砂颗粒的形状分析). *Rock and Soil Mechanics*, pp. 1389-1392. https://doi.org/10.16285/j.rsm.2005.09.008

[17] Zhang, H., Ren, Y., Ge, H., (2019). Review and Prospect of Research on Particle Shape (颗粒形状的研究综述与展望). *Heilongjiang Science*, Vol.10, pp.16-19. https://doi.org/10.3969/j.issn.1674-8646.2019.22.005

[18] Xu, F. (2002). Study on Evaluation Method of Particle Shape of Coarse Aggregate (粗骨料颗粒形状评定方法的研究). *Journal of Yangzhou University (Natural Science Edition)*, pp. 61-63. https://doi.org/10.19411/j.1007-824x.2002.02.016

[19] Kong, L., Peng, R., (2011). Influence of Particle Shape on Mechanical Properties of Sand-like Soil Based on Particle Flow Simulation (颗粒形状对类砂土力学性质影响的颗粒流模拟). *Chinese Journal of Rock Mechanics and Engineering*, Vol. 30, pp. 2112-2119.

[20] Hou, Z., Dai, N., Chen, Z., Chou, Y., Zhang, Y., (2020). Determination of Physical Properties Parameters and Calibration of Discrete Element Simulation Parameters for Crested Wheatgrass Seeds (冰草种子物性参数测定与离散元仿真参数标定). *Transactions of the Chinese Society of Agricultural Engineering*, Vol. 36, pp. 46-54. https://doi.org/10.11975/j.issn.1002-6819.2020.24.006

[21] Chen, Z., Che, G., Wan, L., Wang, H., Zhang, K., (2025). Calibration and Experimental Validation of Discrete Element Parameters for Long-Grain Rice with Different Moisture Contents Based on Repose Angle. *Agriculture*, Vol. 15, pp. 1058-1058. https://doi.org/10.3390/AGRICULTURE15101058

[22] Jian, Z., Li, C.,Niu, Q., Wang, P., Wang, L., Li, H., (2023). Characterization of Green Peppers Based on Dynamic Repose Angle. *LWT*, Vol. 180. https://doi.org/10.1016/J.LWT.2023.114703